Study of electronic and magnetic properties and related x-ray absorption spectroscopy of ultrathin Co films on BaTiO₃

M Hoffmann[1,2], **St Borek**[3], **I V Maznichenko**[1], **S Ostanin**[2], **G Fischer**[4], **M Geilhufe**[2], **W Hergert**[1], **I Mertig**[1,2], **A Ernst**[2] and **A Chassé**[1]

[1] Institut für Physik, Martin-Luther-Universität Halle-Wittenberg, D-06099 Halle, Germany
[2] Max-Planck Institut für Mikrostrukturphysik, Weinberg 2, D-06120 Halle, Germany
[3] Department Chemie, Ludwig-Maximilians-Universität München, Butenandtstraße 11, D-81377 München, Germany
[4] Institut National des Sciences Appliquées Toulouse, LPCNO, 135 Avenue de Rangueil, 31077 Toulouse, France

E-mail: angelika.chasse@physik.uni-halle.de

CrossMark

Abstract

We present a first-principles study of electronic and magnetic properties of thin Co films on a BaTiO₃(0 0 1) single crystal. The crystalline structure of 1–3 monolayer thick Co films was determined and served as input for calculations of the electronic and magnetic properties of the films. The estimation of exchange constants indicates that the Co films are ferromagnetic with a high critical temperature, which depends on the film thickness and the interface geometry. In addition, we calculated x-ray absorption spectra, related magnetic circular dichroism (XMCD) and linear dichroism (XLD) of the Co $L_{2,3}$ edges as a function of Co film thickness and ferroelectric polarization of BaTiO₃. We found characteristic features, which depend strongly on the magnetic properties and the structure of the film. While there is only a weak dependence of XMCD spectra on the ferroelectric polarization, the XLD of the films is much more sensitive to the polarization switching, which could possibly be observed experimentally.

S Online supplementary data available from stacks.iop.org/JPhysCM/27/426003/mmedia

(Some figures may appear in colour only in the online journal)

The interface between a magnetic thin film and a ferroelectric material is the subject of several recent investigations [1–19]. The major part of these studies is devoted to Fe/ferroelectric interfaces [2, 4–7, 10, 12, 14–18], since ferromagnetic iron is supposed to be a good candidate as a ferromagnetic electrode in two-component multiferroics. Although it was shown, that a ferroelectric film can be grown on an iron substrate and a functional heterojunction can be fabricated [14, 15], the multiferroic effects by polarization switching were found to be not strong enough, since the main changes of the functional properties occur only in the vicinity of the interface [2, 6, 15]. Another impediment is non-ideal compatibility between an iron and an oxide surface. Until now it was not shown that junctions with symmetric interfaces, a highly desirable condition for coherent electronic transport [20], can be grown. Accordingly, ferromagnetic oxides La₁₋ₓSrₓMnO₃ and SrRuO₃ were used as electrodes in multiferroic junctions [3, 8, 9, 11, 19]. Such interfaces can be almost ideally grown, but the Curie temperature of these oxides is too low for functional devices. Therefore, search for an appropriate ferromagnetic/ferroelectric interface is still in progress.

Among the above cited studies only few investigations deal with ultrathin ferromagnetic films on a ferroelectric substrate [6, 7, 12, 16]. In particular, it was shown that two monolayer

1

TH-2015-39

thick Fe films on the BaTiO$_3$(0 0 1) surface might not be fer-romagnetic because of the film geometry and magneto-elastic properties of iron [6]. Additionally, a substantial charge and spin moment transfer was found at the interface by altering the polarization direction [6].

Thus, ultrathin films of Fe on a BaTiO$_3$(0 0 1) single crystal are magnetically unstable [6], but cobalt exhibits usually stable ferromagnetic characteristics in many nanostructures. Therefore, we continue our work on ultrathin metallic films on ferroelectric single crystals and suggest in this paper to use Co as the ferromagnetic material on BaTiO$_3$(0 0 1).

Despite the comprehensive review about the progress in this field given by Vaz *et al* [21] there are only few informa-tion about the interface of Co and perovskites like BaTiO$_3$ (BTO). In the framework of spin-polarized DFT calcula-tions, as implemented in the Vienna *ab initio* Simulation Package (VASP), multiferroic tunnel junctions of Co/BTO/ Co were investigated by Cao *et al* [13]. They showed that a critical thickness of BTO unit cells is necessary for the appearance of ferroelectricity, which is inhibited by a depo-larizing electrostatic field, caused by dipoles at the ferro-electric-metal interfaces [22]. In the work of Oleinik *et al* [23], first-principles calculations were applied on Co/STO/ Co(0 0 1) magnetic tunnel junctions, where a strong covalent bond between Co and O and an induced magnetic moment of $|m_s| = 0.25\,\mu_B$ at the Ti atom was observed. This is similar to the case of Fe/BTO/Fe tunnel junctions. In another work, Polisetty *et al* [24] applied piezoelectrically controlled strain for electric tuning of exchange-bias fields of BTO/Co/CoO heterostructures.

In our first-principles study, we investigated systematically the crystalline structure of ultrathin Co films on BTO and their electronic and magnetic properties in dependence on the film thickness and the polarization of BTO. The calculations were performed using a so-called multi-code approach, in which atomic positions were obtained using a pseudo-potential code, VASP [25, 26]. This information serves as input for electronic and magnetic structure calculations with different multiple-scattering Green function methods [27–29].

In addition, we simulated x-ray absorption spectra (XAS) and the related x-ray magnetic circular dichroism (XMCD), which is the method of choice to prove experimentally the change of the magnetic structure. The x-ray linear dichroism (XLD) is dicussed in respect of the occupation of *d* orbitals. These methods are local and site-sensitive and offer the opportunity to investigate both the magnetic and structural properties as a function of layer thickness [16]. So, we traced the dependence of XAS of Co $L_{2,3}$ edges as a function of the Co film thickness and the polarization direction of BTO. All results were compared with the previous results for Fe thin films on BTO [6, 16].

Our paper is organized as follows. Our multi-code approach and computational details are presented in the next section 1. Then, in sections 2 and 3, we discuss structural, electronic, and magnetic properties of ultrathin Co films on BTO. Sections 4 and 5 deal with computational simulations of XAS, XMCD, and XLD spectra. Conclusion is offered in section 6.
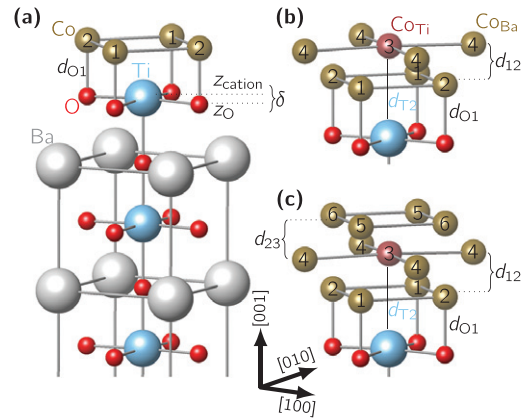

Figure 1. Geometry of Co films on the BaTiO$_3$ surface for 1 ML (a), 2 ML (b), and 3 ML (c) cobalt thicknesses, respectively. Spheres represent Co (brown), Ba (gray), Ti (blue), and oxygen (red) sites. The values of selected interatomic distances for polarizations $\boldsymbol{P} = P_\downarrow, P_\uparrow$ are presented in table 1. The picture of the underlying structure was done with VESTA [41]. The numbers for the Co atoms symbolize the atoms of the unit cell and correspond to those in the figures of the supplementary material stacks.iop.org/ JPhysCM/27/426003/mmedia.

1. Computational details

1.1. Structural optimization

The information about the crystalline structure of Co/BTO(0 0 1) was obtained using projector-augmented wave pseudo-potentials [30] implemented in the VASP code [25, 26]. The plane-wave basis was taken with a cutoff energy of 400 eV. The calculations were performed within the local spin-density approximation (LSDA). We used the parametri-zation of Perdew and Wang for the exchange-correlation func-tional (PW-functional) [31]. Here, we believe that the impact of electronic correlations on the interface magnetoelectric coupling is minor.

We performed the structural optimization of Co/BTO(0 0 1) in dependence on the Co film thickness and the ferroelectric polarization $\boldsymbol{P}$ of BTO(0 0 1). To model the (0 0 1) surface of polar BTO, we constructed a 5 unit cells (~ 2 nm) thick super-cell, with a vacuum spacer of 2 nm along the [0 0 1] direction. The lattice parameters were set to the theoretical equilibrium values of tetragonal BTO [6]: $a = 3.943$ Å and $c/a = 1.013$. The intralayer cation-oxygen displacements $\delta = z_O - z_{cation}$ (see figure 1) in BTO cause the ferroelectric polarization, $\boldsymbol{P}$, along [0 0 1]. When $\boldsymbol{P}$ is antiparallel to the surface normal ($P_\downarrow$), the oxygen in each monolayer (ML) are higher then the cations ($\delta > 0$), and *vice versa*, the ferroelectric state $P_\uparrow$ means $\delta < 0$. Since the (0 0 1) surface of BTO is TiO$_2$ terminated [6] for both directions of $\boldsymbol{P}$, the Co atoms find their relaxed positions atop the oxygen atoms. This is in agreement with the recent experimental data for Fe/BTO(0 0 1) [14]. Each Co monolayer of the slab contains, therefore, two atoms per unit cell while the Co film thickness, L, varies between one and three ML. For Co/BTO(0 0 1) the atomic positions of the four top BTO layers and all Co ML were allowed to relax. After the relaxa-tion, the calculated forces are always less than 0.5×10^{-2}

eV Å^{-1}. The Brillouin zone of the slab was sampled with a $10 \times 10 \times 6$ k-point Monkhorst-Pack mesh [32] during the force minimization.

1.2. Electronic and magnetic structure calculations

The relaxed geometry was used for further first-principles calculations using the Korringa–Kohn–Rostoker Green function method (KKR) [33, 34] called HUTSEPOT. HUTSEPOT is developed by Ernst *et al* at the Max Planck Institute of Microstructure Physics, Germany. Some of its basic features are described in [27].

We took within the atomic sphere approximation to the crystal potential an angular momentum cutoff of $l_{\max} = 3$ for the Green function, a k-point mesh of $24 \times 24 \times 12$ for the BZ integration and 24 Gaussian quadrature points for complex energy contour integration. With the Green function $G(E)$ of the system, all quantities of interest follow in a straightforward way. In particular, we are interested in ground state properties like the density of states (DOS) and the local magnetic moments [35] in dependence on Co film thickness L and ferroelectric polarization direction $\boldsymbol{P}$ of BTO.

To describe magnetic properties of Co/BTO(0 0 1), we calculated interatomic exchange coupling parameters J_{ij} using the magnetic force theorem implemented within the Green function method [36]. The exchange coupling constants J_{ij} can be used to obtain spin-wave spectra by the diagonalization of the Heisenberg Hamiltonian

$$H = -\sum_{i \neq j} J_{ij} \boldsymbol{e}_i \boldsymbol{e}_j - \sum_i E_{\text{MAE}} (e_i^z)^2, \tag{1}$$

where i and j label magnetic atoms, $\boldsymbol{e}_i$ is a unit vector in the direction of the magnetic moment of the ith atom and E_{MAE} is the magnetic anisotropy energy (MAE), which is positive (negative) for the case of the easy-axis (easy-plane) anisotropy type. It can be calculated directly with the KKR method by using again the magnetic force theorem [37]. The critical temperatures were estimated using a Monte Carlo (MC) simulation with the model Hamiltonian in (1). For the simulation, two dimensional supercells, which repeat the unit cell (see figure 1) 60×60, 80×80, and 100×100 times in x and y direction were constructed. In those directions, we considered also periodic boundary conditions and restricted the calculation only to the magnetic atoms of the unit cell (2 Co atoms for $L = 1$, 4 Co atoms for $L = 2$, and 6 Co atoms for $L = 3$). Within the supercell, the magnetic moment at lattice site i interacts with its neighbors at the site j via the first-principles J_{ij}. During a MC run, a lattice site j with the magnetic moment vector $\boldsymbol{e}_j$ was chosen and a new random direction $\boldsymbol{e}'_j$ was created. The energy of the system determines whether $\boldsymbol{e}'_j$ or $\boldsymbol{e}_j$ was kept. Performing this procedure N times on a lattice of N sites is defined as one MC step. The starting point was a high-temperature disordered state above the critical temperature T_{C}. In the course of the simulations, the temperature was stepwise reduced until magnetic ordering was reached. For each temperature T, the thermal equilibrium was assumed to be reached after 20 000 MC steps. The thermal averages

Table 1. Relaxed interatomic distances (in Å) of $(\text{Co})_L/\text{BTO}(0\,0\,1)$ ($L \leqslant 3$ and $\boldsymbol{P} = P_\downarrow, P_\uparrow$).

		Co		Fe	
		$P_\downarrow$	$P_\uparrow$	$P_\downarrow$	$P_\uparrow$
$L = 1$	d_{O1}	1.778	1.784	1.774	1.781
$L = 2$	d_{O1}	1.856	1.853	1.857	1.855
	d_{12}	1.116	1.107	1.049	1.054
	d_{T2}	3.022	2.927	2.971	2.918
$L = 3$	d_{O1}	1.827	1.829	1.843	1.849
	d_{12}	1.183	1.179	1.218	1.241
	d_{23}	1.154	1.153	1.134	1.114
	d_{T2}	3.094	3.014	3.214	3.121
bulk (hcp):			2.478		

Note: For each L, the distances between Co ML i and j are denoted by d_{ij} while the z-separation from interfacial O (Ti) to Co of the first (second) ML is shown by d_{O1} (d_{T2}). For comparison, also nearest neighbor Co distances in bulk (hcp) [45] and distances for $(\text{Fe})_L/\text{BTO}(0\,0\,1)$ are shown.

were determined over 20 000 additional MC steps. T_{C} was then obtained from the temperature dependency of the magnetic susceptibility. With respect to fitting procedures and finite temperature sampling, all three supercells yielded the same critical temperature within an uncertainty range of ± 5 K. More details of our MC scheme can be found in [38–40].

1.3. X-ray absorption spectra simulations

Using the self-consistent potentials of HUTSEPOT, the calculations were extended to a spin-resolved fully relativistic KKR code (SPR-KKR) [29]. This Green function method [29] allows the calculation of x-ray absorption coefficients $\mu^\lambda(E)$ in dependence on the energy E and the polarization λ of the x-rays [42–44]. For SPR-KKR calculations of magnetic moments, XAS and DOS, we have taken 144, 578 and 225 k-points in the irreducible part of the Brillouin zone, respectively. The calculation of the structure constants were done using the Ewald method with parameter 2.0 and 4.0 in real space and reciprocal space, respectively. For the Ewald parameter connecting the summation in real and reciprocal space a value of 0.8 was used, making the summation in the real space converge faster. These parameters were applied for all considered Co/BTO systems.

2. Crystalline structure of ultrathin Co films on BTO

For the ultrathin Co films deposited on BTO(0 0 1), the optimized interatomic distances are collected in table 1, in comparison with the corresponding structure of Fe/BTO(0 0 1) [6, 16]. The definition of our distances are given in figure 1. Below in the text, the interface TiO_2 layer is denoted as I for all films. The Co layers towards the surface are labeled with $\text{I} + 1$, $\text{I} + 2$, and $\text{I} + 3$.

Structural relaxation, with the in-plane degrees of freedom for the layers starting with $\text{I} - 2$, energetically favors the structure with the Co sites in layer $\text{I} + 1$ on top of the O sites in layer I. In the case of 1 ML Co ($L = 1$), the structure is similar to that of Fe/BTO(0 0 1) [6, 16]. For both multiferroic

Table 2. SPR-KKR results of magnetic spin moments m_s (μ_B/atom) for (Co)$_L$/BTO(0 0 1) in dependence on the Co film thickness L and the direction of ferroelectric polarization $\boldsymbol{P}$ ($\boldsymbol{M} \parallel$ [0 0 1]).

		$L = 1$		$L = 2$		$L = 3$	
		$P_\downarrow$	$P_\uparrow$	$P_\downarrow$	$P_\uparrow$	$P_\downarrow$	$P_\uparrow$
Co	I + 3					1.39	1.42
Co$_{Ba}$	I + 2			2.00	2.03	1.60	1.64
Co$_{Ti}$	I + 2			1.89	1.93	1.45	1.47
Co	I + 1	1.71	1.71	1.62	1.62	1.42	1.37
O	I	0.08	0.08	0.03	0.03	0.06	0.05
Ti	I	−0.11	−0.18	−0.12	−0.16	−0.03	−0.08
Co bulk (hcp):		1.62					

Note: The Co labels follow from figure 1. In I + 1 and I + 3 the Co atoms are equivalent.

systems, the polarization state $P_\downarrow$ results in a slightly shorter distance, d_{OI}, between Co (Fe) and interfacial O.

When the Co film thickness increases to $L = 2$ and 3, a distorted bodycentered tetragonal (bct) lattice is formed, although it is not typical for Co [21]. We found that the polarization reversal affects mainly the positions of interfacial Ti (I) and consequently those of the Co (I + 2) atoms, labeled as Co$_{Ba}$ and Co$_{Ti}$, respectively (see figure 1). This is important concerning the magnetic properties of the films.

3. Electronic and magnetic properties of ultrathin Co films on BTO

In order to determine the magnetic ground state for the three film thicknesses, we calculated the total energy for the ferromagnetic (FM) and antiferromagnetic (AFM) configurations of the magnetic moments of the Co atoms. In all cases, the FM solution was preferable, independent of thickness or polarization. So, the thin cobalt films are strong ferromagnets and show a lower sensitivity to structural transformations than the iron layers, which showed a considerable change in the magnetic order for different layer thicknesses. For the 2 ML Fe film on BTO, the m_{Fe} in layer I + 1 were almost quenched while the sizable moments in the surface layer I + 2 are ordered antiparallel. This results in a total magnetic moment of $m \rightarrow 0$. Deposition of a third Fe monolayer restored the ferromagnetic order of the 1 ML Fe film.

3.1. Magnetic moments and density of states

The calculated spin moments (see table 2) for the Co atoms show a strong dependence on the geometry of the films and the hybridization of Co 3d states with the electronic bands of the substrate. The different environment of e.g. Co$_{Ba}$ and Co$_{Ti}$, in particular, the atomic volumes and the band hybridization, influences also these moments.

In the case of $L = 1$ and $L = 2$, the spin moments for Co atoms at the surface, are larger then for the Co bulk (hcp) because of the symmetry reduction and an enhanced volume per Co atom. The Co magnetic moments in layer I + 1 for $L = 2$
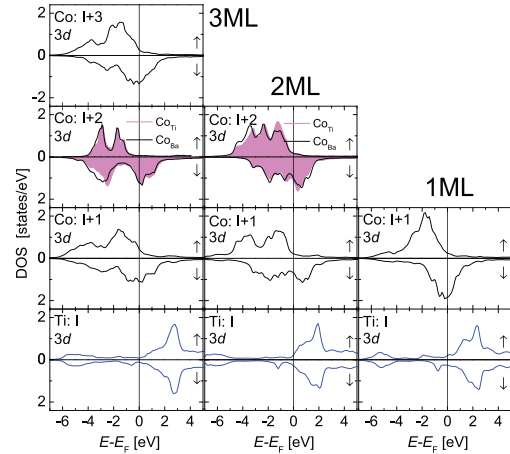
Figure 2. Spin-resolved (↑,↓) density of d states for Co and Ti atoms in dependence on film thickness L. It is only shown for $P_\uparrow$, because there are only small differences for $P_\downarrow$.

Table 3. SPR-KKR results of magnetic orbital moments m_o (μ_B/atom) for (Co)$_L$/BTO(0 0 1) in dependence on the Co film thickness L and the direction of ferroelectric polarization $\boldsymbol{P}$ ($\boldsymbol{M} \parallel$ [0 0 1]).

		$L = 1$		$L = 2$		$L = 3$	
		$P_\downarrow$	$P_\uparrow$	$P_\downarrow$	$P_\uparrow$	$P_\downarrow$	$P_\uparrow$
Co	I + 3					0.09	0.08
Co$_{Ba}$	I + 2			0.08	0.08	0.07	0.07
Co$_{Ti}$	I + 2			0.09	0.08	0.07	0.07
Co	I + 1	0.17	0.17	0.07	0.06	0.09	0.09
Co bulk (hcp):		0.06					

Note: The Co labels follow from figure 1. In I + 1 and I + 3 the Co atoms are equivalent.

approach their bulk value. For $L = 3$, the spin moments of Co (I + 1) and Co$_{Ti}$ are smaller in comparison to $L = 2$, because of slightly elongated distances d_{12} and d_{T2}, respectively. In the case of $L = 3$, we observe for all three layers a quenching of the spin moment in comparison to Co bulk (hcp), which results from a strong reduction of the volume per Co atom.

Besides, we also observe induced magnetic moments at the Ti and O atoms at the interface (see table 2). For the Ti atoms, these induced magnetic moments are antiparallel oriented to the direction of the magnetic moments of the Co atoms and are originated, similar to the case of Fe/BTO(0 0 1), from the hybridization of Ti and Co 3d states (see figure 2). The strong interaction between the host and the Co films widens the DOS of the layers at the interface, while the 3d states of Co become very narrow towards the surface, which results from the reduced coordination number of Co atoms at the surface (in comparison to Co bulk). The impact of the crystalline environment is very strong on the DOS and the magnetic moments of the Co atoms. As a result, the magnetic moments on Co$_{Ti}$ are smaller by 0.08 μ_B–0.15 μ_B then on Co$_{Ba}$(I + 2) due to the strong interaction between the Co$_{Ti}$ and the Ti states. A short distance between Co(I + 3) and Co(I + 2) and a strong Co-Co hybridization in the case

Table 4. SPR-KKR results of magnetic orbital moments m_o (μ_B/atom) with $\boldsymbol{M} \parallel [1\,0\,0]$.

		L = 1		L = 2		L = 3	
		$P_\downarrow$	$P_\uparrow$	$P_\downarrow$	$P_\uparrow$	$P_\downarrow$	$P_\uparrow$
Co$_6$	I + 3					0.12	0.07
Co$_5$	I + 3					0.07	0.11
Co$_4$	I + 2			0.12	0.12	0.07	0.07
Co$_3$	I + 2			0.12	0.13	0.06	0.06
Co$_2$	I + 1	0.16	0.12	0.08	0.08	0.06	0.04
Co$_1$	I + 1	0.13	0.17	0.07	0.06	0.07	0.05

Note: The Co labels follow from figure 1. In this field direction the Co atoms are nonequivalent.
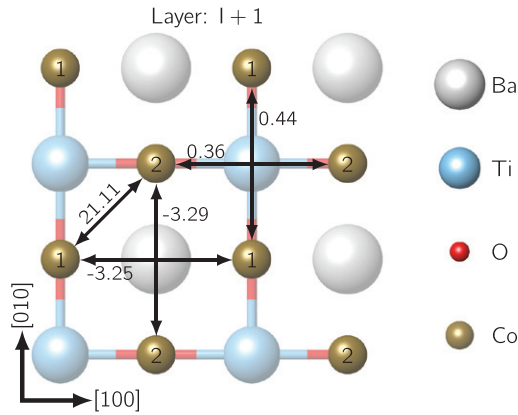
Figure 3. Calculated intralayer exchange constants (in meV) for layer I + 1 in 1 ML Co/BTO(0 0 1) and $P_\uparrow$, viewed from the z direction. Atoms in lighter colors are below those in darker colors. The numbers of the Co atoms correspond to those used in figure 1(a).

Figure 4. Calculated exchange constants (in meV) for 2 ML Co/BTO(0 0 1) and $P_\uparrow$. The notation is the same as in figure 3 and the numbers of the Co atoms correspond to those used in figure 1(b). Intralayer interactions in layers I + 1 and I + 2 are separated from the interlayer interactions shown in the side view. The dashed lines in the two upper panels indicate the Co atoms shown in the side view. For symmetric interactions only one number is given.

of $L = 3$ leads to a substantial reduction of the magnetic moments in the surface Co layer.

We have calculated the orbital moment of Co atoms along $\boldsymbol{M} \parallel [0\,0\,1]$ (see table 3) and along $\boldsymbol{M} \parallel [1\,0\,0]$ (see table 4). In the last case, the two Co atoms in each layer are nonequivalent. In the surface layer the atoms show a strong dependence on the electric polarization of the substrate. For $\boldsymbol{M} \parallel [0\,0\,1]$ the influence of the polarization is weak and is as large as for the Fe/BTO system [16].

Duan *et al* [46] predicted that the magnetic anisotropy of thin magnetic films may be effected by the polarization of the ferroelectric substrate. His calculations done for 1 ML Fe/BTO gave differences for the orbital magnetic moment $\Delta m_o = m_o[0\,0\,1] - m_o[1\,0\,0]$ of 0.035 μ_B and 0.021 μ_B for $P_\uparrow$ and $P_\downarrow$, respectively. In our former work of 1 ML Fe/BTO, we found also an averaged anisotropy of the orbital magnetic moment Δm_o of 0.04 μ_B and 0.06 μ_B (note that there are two Fe atoms in the unit cell of 1 ML Fe) [16]. In case of 1 ML Co/BTO, we get the averaged $\Delta m_o = 0.04$ μ_B for the polarization $P_\uparrow$, which is similar to 1 ML Fe/BTO. There was no strong dependence on the polarization on the BTO substrate in our calculations. The anisotropies for the orbital moment will influence the preference of the easy axis of the magnetization as discussed in the next section.
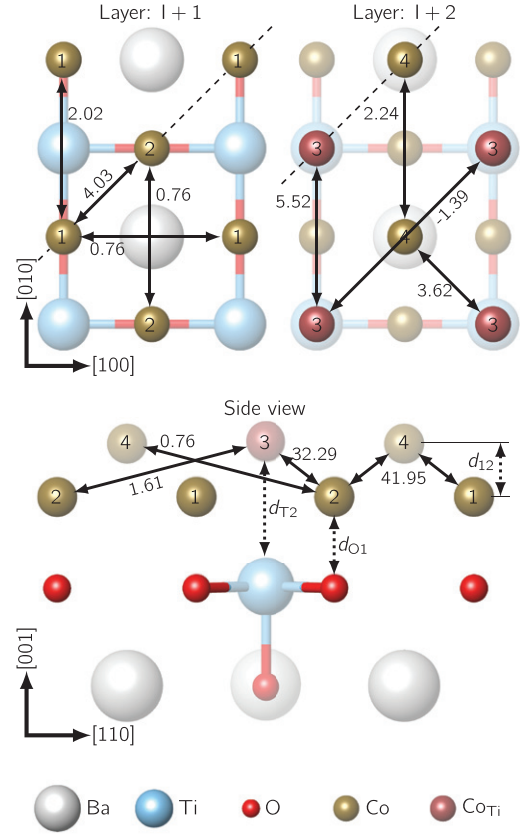
On the other hand, for thicker Co films, the electronic structure can be strongly affected by a Schottky barrier, which develops at a semiconductor–metal interface and can lead to a spurious charge transfer across the interface [47]. However, in very thin metallic films on a semiconductor, the Schottky barrier is not significant and can not substantially modify their electronic and magnetic structure.

3.2. Magnetic interactions and Curie temperatures

To study the magnetic interactions in ultrathin Co films on BTO(0 0 1), we computed the exchange constants, which enter the Heisenberg model (1). The most significant magnetic exchange interactions for Co/BTO(0 0 1) are shown in figures 3–5 for $L = 1, 2, 3$ ML, respectively, while for the sake of completeness all calculated coupling constants are presented in the supplementary material stacks.iop.org/JPhysCM/27/426003/mmedia. They are always separated in interlayer and intralayer contributions.

The key feature of the elaborated results is a very strong magnetic coupling between the nearest neighbors. This means for the 1 ML Co film the in-plane nearest neighbor coupling is about 21 meV (see figure 3; nearest neighbor Co distance
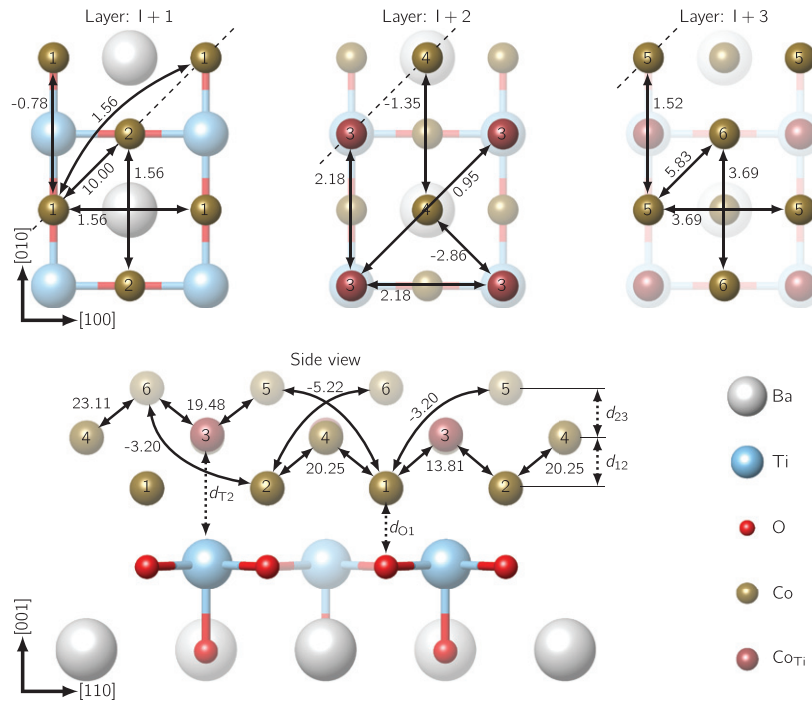
Figure 5. Calculated exchange constants (in meV) for 3 ML Co/BTO(0 0 1) and $P_\uparrow$. The notation is the same as in figure 3 and the numbers of the Co atoms correspond to those used in figure 1(c). Intralayer interactions in the three layers I + 1, I + 2 and I + 3 are separated from the interlayer interactions shown in the side view. The dashed lines in the three upper panels indicate the Co atoms shown in the side view. For symmetric interactions only one number is written (see text).

is 2.79 Å). In this case, the electronic density is mainly distributed within the *xy*-plane and the exchange integrals represent an overlap between the electronic wave functions. Hence, comparing with Co bulk (hcp) the magnetic coupling in 1 ML remains stronger despite the larger nearest neighbor distance (in Co bulk (hcp) the nearest neighbor magnetic coupling is ≈ 13 meV).

In contrast, for the films with an out-of-plane component (2 ML, 3 ML), the distances towards the Co atoms in the next layer are shorter (2.23 Å). Therefore, the nearest neighbor coupling is now between those layers and the wave function overlap is even stronger. It leads to a strong magnetic interaction between 32 meV–42 meV for 2 ML (see figure 4). In the case of 3 ML, the electronic density redistributes in all directions and, therefore, the strength of the interlayer exchange interactions with respect to those of 2 ML is reduced to 13 meV–20 meV (see figure 5). Comparing these results with the exchange constants in Co bulk, we found in general a strong asymmetry between in-plane and out-of-plane components. The latter are larger while the in-plane directions are strongly reduced (see figures 4 and 5).

Furthermore, we obtain a partial mediation of the magnetic coupling by the BTO host. The exchange interaction between e.g. the second nearest neighbor Co atoms depends on the underlying atoms, either ≈ −3.3 meV or ≈ 0.4 meV with mediating Ba or Ti, respectively (see figure 3). This fact can also be observed for 2 and 3 ML (see figures 4 and 5) and is evident from the comparison of the calculated J_{ij} for

supported and unsupported thin Co films, shown in the supplementary material stacks.iop.org/JPhysCM/27/426003/mmedia. While using the same geometry for the Co films, we removed the BTO substrate in the calculations. Immediately, the symmetry of *x* and *y* directions returns and some exchange interaction values differ more than 10 meV.

For the Monte Carlo simulations with the classical Heisenberg Hamiltonian (1), we have also computed the magneto-crystalline anisotropy energy (MAE) $E_{MAE} = E_{[0\,0\,1]} - E_{[1\,0\,0]}$ for various Co thicknesses and polarizations (see table 5). We found an out-of-plane magnetization direction for the cases of 1 and 3 ML Co/BTO(0 0 1), while in the case of 2 ML Co/BTO(0 0 1), the magnetization direction is in-plane. The change in the MAE with the polarization switch can reach up to 25%–30%. It is remarkable, that in the 2 ML Co case, the magnetization direction is lying within the *xy*-plane, which can be explained by the small interlayer distance (see table 1).

These MAE values were then used together with the calculated J_{ij} parameters to determine the critical temperatures T_C in dependence on the layer thickness *L* and polarization **P**. In general, the thin $(Co)_L$/BTO films are ferromagnetic at room temperature for $L \geqslant 2$ (see table 5). However, as expected from the large variations of the magnetic coupling parameters, the T_C increase not monotonically with the thickness. The main contributions in the magnetic exchange originate from the strong interlayer coupling. The different polarization directions have only a small influence to the value of T_C, which follows from the similar J_{ij} parameters for $P_\uparrow$ or $P_\downarrow$ (for all values see the supplementary material stacks.iop.org/JPhysCM/27/426003/

Table 5. Magnetic anisotropy energy and critical temperature for $(Co)_L/BTO(0\,0\,1)$ in dependence on the Co film thickness L and the direction of ferroelectric polarization $\boldsymbol{P}$.

|	E_{MAE} (meV)		T_C (K)	
L	$P_\downarrow$	$P_\uparrow$	$P_\downarrow$	$P_\uparrow$
1	-1.847	-1.483	360 (307)	298 (250)
2	0.680	0.958	844 (820)	818 (780)
3	-0.270	-0.438	567 (550)	580 (550)

Note: T_C in brackets is for $E_{MAE} = 0$ meV.
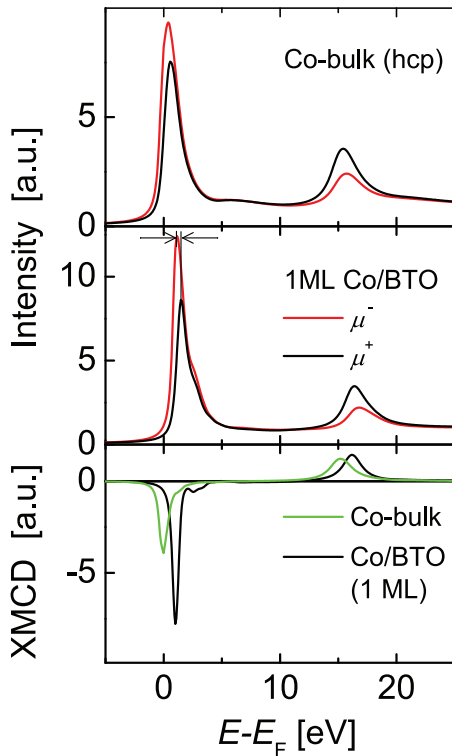
Figure 6. Calculated XAS (upper and middle part) and XMCD (lower part) of 1 ML Co on BTO(0 0 1) $(P_\uparrow)$ in comparison to Co bulk (hcp). Open arrows indicate difference in peak position (see text).

mmedia). As expected, a value for MAE $(E_{MAE} \neq 0)$ increases the Curie temperature (see table 5).

4. XAS and XMCD

The Co $L_{2,3}$ edges are in the focus of our XMCD discussion. We have calculated x-ray absorption spectra of right- and left-circular polarized x-ray radiation in dependence on the Co film thickness L and the electric polarization direction $\boldsymbol{P}$ of BTO. The difference of the absorption coefficients $\Delta\mu = \mu^+(E) - \mu^-(E) \equiv$ XMCD is normalized to the number of Co atoms in the monolayers. All x-ray absorption spectra were broadened by Lorentz convolution with a core hole width of 0.9 eV and 0.25 eV for the L_2 and L_3 edge, respectively. In our simulations of XAS and XMCD the magnetization $\boldsymbol{M}$, the electric polarization $\boldsymbol{P}$ and the incidence of light are parallel to the z-axis (surface normal) of the Co/BTO(0 0 1) system.
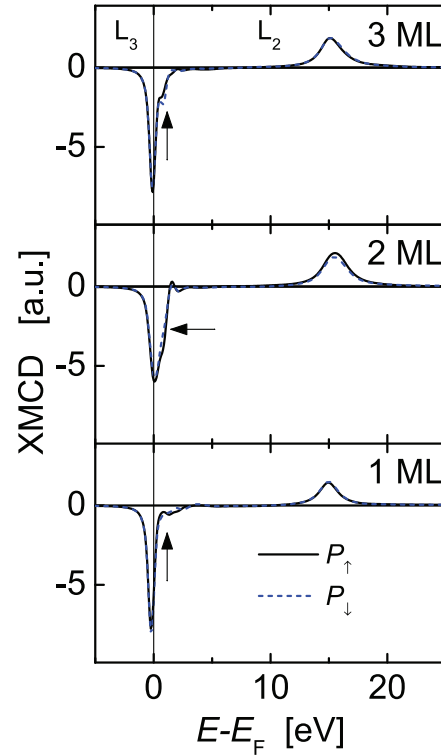
Figure 7. Calculated XMCD of Co $L_{2,3}$ edges in Co/BTO in dependence on film thickness and electric polarization $\boldsymbol{P}$ of BTO ($P_\uparrow$ solid lines, $P_\downarrow$ dotted lines). Arrows indicate different small features (see text). The thin vertical line visualizes the difference in the peak positions.

In figure 6 the calculated x-ray spectra $\mu^\pm(E)$ (upper part) and the related difference spectra (lower part) for 1 ML Co/BTO(0 0 1) $(P_\uparrow)$ are compared to calculations performed for Co bulk (hcp). The results of our XMCD calculations for $(Co)_L/BTO$ with $L = 1, 2, 3$ and $P_\uparrow$ and $P_\downarrow$ are summarized in figure 7.

In all cases, we observe the well-known energy dependence of XMCD, where the intensity μ^+ at the L_3 (L_2) edge is decreased (enhanced) due to different selection rules of spin-up and spin-down electrons in the ferromagnetic phase. The behavior is opposite at the L_3 (L_2) edge in case of μ^-. The dependence on the electric polarization $\boldsymbol{P}$ of BTO is in all cases very weak (see dotted lines in figure 7).

In comparison to Co bulk, we found small but significant differences concerning ultrathin films. Note that the maxima of the L edges of left and right circularly polarized light are not at the same energetic position as observed for Co bulk XAS (see open arrows in figure 6). This can be attributed (as in the case of Fe/BTO [16]) to the cancellation of degenerate d states at the interface and/or surface of the film.

In the energy dependence of the L_3 edge, we observe a small structure of the XMCD peak at higher energy (see closed arrows in figure 7) in dependence on layer thickness. The appearance of this structure can also be explained if we consider the layer-resolved XMCD (not shown here) as demonstrated for the system Fe/BTO [16]. In general, it is possible to separate all the different contributions by means of
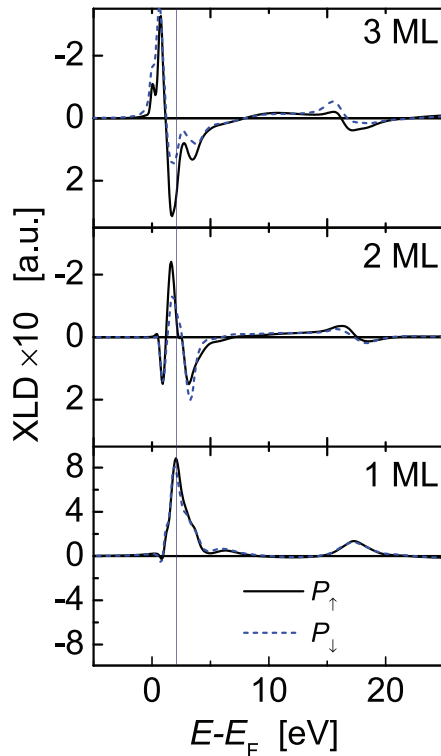
Figure 8. Calculated XLD of Co $L_{2,3}$ edges in Co/BTO for polarization **P** ($P_\uparrow$ solid lines, $P_\downarrow$ dashed lines). The thin vertical line visualizes the difference in the peak positions.

layer-resolved XMCD calculations. This dependence on layer thickness should show up in corresponding experiments.

5. X(M)LD

X-ray absorption linear dichroism can be applied in different modes [48]. In nonmagnetic materials with cubic symmetry the x-ray absorption intensity is independent of the orientation of the polarization vector of light (**u**) relative to the sample. As the symmetry is lowered (like in a film), the intensity is directly proportional to the number of empty valence states in the direction of **u**. The vector **u** acts like a search light for the direction of maximum and minimum empty valence states [48]. In case of a magnetic sample with cubic symmetry, the spin–orbit coupling leads to magnetic linear dichroism, where the x-ray absorption intensity is different for **u** aligned parallel and perpendicular to the spin direction [43]. This kind of dichroism is often considered in the discussion of magneto-crystalline effects (e.g. [49]).

In our magnetic ultrathin Co films on BTO, we have both natural and magnetic linear dichroism effects. First, we present results for a fixed direction of magnetization **M**∥[0 0 1] and linearly polarized light with polarization along [0 0 1] (μ^z) and [1 0 0] (μ^x), respectively. The difference XLD $= \mu^z(E) - \mu^x(E)$ between both x-ray absorption spectra is shown in figure 8.

The strong dependence of the XLD on the film thickness can be related to the occupation of d orbitals. A detailed analysis is possible concerning the single (p_j, m_j) contributions of the

initial $p_{3/2}$ ($p_{1/2}$) state to the $p \to d$ transitions of the different Co absorbers in the film. In the 1 ML case, we get the main positive contribution from the transition of $m_j = -1/2$ into $d_{3z^2-r^2}$ states. The contributions of d_{xz} and d_{yz} are small because of the strong interaction between Co and Ti atoms at the interface. The XLD of 2 ML reflects the change of occupancy between in-plane and out-of-plane orbitals. In the 3 ML case, we found that the behavior is similar to the Co bulk, but with much more fine structures. These fine structures are related to the lifting of degeneracy in the final d state in the thin film.

Besides, we found that the XLD is much more sensitive concerning the dependence on the polarization of the BTO substrate as the XMCD. This emphasize how the reversal of polarization **P** changes the occupation of d states.

We have also investigated x-ray absorption in dependence on the magnetization direction **M** for fixed vector **u**∥[0 0 1] but spin–orbit interaction and crystal field are both to weak to eliminate magneto-crystalline anisotropy.

6. Conclusion

In this first-principles study of structural, electronic, and magnetic properties of ultrathin Co layers on the BaTiO$_3$(0 0 1) substrate, we showed, that the crystalline structure of (Co)$_L$/BTO(0 0 1) ($L = 1, 2, 3$) interfaces is very similar to the one of (Fe)$_L$/BTO(0 0 1) films presented in our previous study [6]. Additionally, we found also for the Co layers only a small dependence on the polarization direction of the substrate for all investigated properties. However, in contrary to the Fe/BTO(0 0 1) case, Co films on BTO(0 0 1) exhibit a stable ferromagnetic ordering at room temperature, which depends strongly on the layer thickness and is the strongest for $L = 2$. The magnetic interaction is mainly featured by the coupling between the nearest neighbors. For $L \geqslant 2$ cases, the strongest interactions arise between the adjacent layers, while the intra-layer magnetic coupling was found to be rather weak. This results from short interlayer distances leading to a strong hybridization between Co 3d electrons of adjacent layers. Surprisingly, the easy axis turns for 2 ML from a out-of-plane magnetization (in $L = 1$ and 3) to a in-plane magnetization, which was obtained from the direct calculation of the MAE or the calculated orbital moments.

For a comparison to possible experimental measurements, we simulated x-ray absorption spectra and related x-ray magnetic circular and (magnetic) linear dichroism to trace the change of the spectra under the polarization switching in the BTO substrate. While the XMCD depends only weakly on the substrate polarization, similar to our previous study for Fe$_L$/BTO(0 0 1) films [16], the XLD shows indeed significant changes under polarization switching, which can probably be observed experimentally.

Acknowledgments

'Functionality of Oxide Interfaces'. The authors would like to thank Jan Minár and Hubert Ebert for deployment and support of the SPR-KKR program and helpful discussions.

References

[1] Tsymbal E Y and Kohlstedt H 2006 *Science* **313** 181
[2] Duan C G, Jaswal S S and Tsymbal E Y 2006 *Phys. Rev. Lett.* **97** 047201
[3] Duan C G, Sabirianov R F, Mei W N, Jaswal S S and Tsymbal E Y 2006 *Nano Lett.* **6** 483
[4] Sahoo S, Polisetty S, Duan C G, Jaswal S S, Tsymbal E Y and Binek C 2007 *Phys. Rev.* B **76** 092108
[5] Velev J P, Duan C G, Belashchenko K D, Jaswal S S and Tsymbal E Y 2008 *J. Appl. Phys.* **103** 07A701
[6] Fechner M, Maznichenko I V, Ostanin S, Ernst A, Henk J, Bruno P and Mertig I 2008 *Phys. Rev.* B **78** 212406
[7] Fechner M, Ostanin S and Mertig I 2009 *Phys. Rev.* B **80** 094405
[8] Gruverman A *et al* 2009 *Nano Lett.* **9** 3539
[9] Niranjan M K, Burton J D, Velev J P, Jaswal S S and Tsymbal E Y 2009 *Appl. Phys. Lett.* **95** 052501
[10] Garcia V *et al* 2010 *Science* **327** 1106
[11] Vaz C A F, Hoffman J, Segal Y, Reiner J W, Grober R D, Zhang Z, Ahn C H and Walker F J 2010 *Phys. Rev. Lett.* **104** 127202
[12] Fechner M, Maznichenko I V, Ostanin S, Ernst A, Henk J and Mertig I 2010 *Phys. Status Solidi* B **247** 1600
[13] Cao D, Cai M Q, Hu W Y and Xu C M 2011 *J. Appl. Phys.* **109** 114107
[14] Meyerheim H L, Klimenta F, Ernst A, Mohseni K, Ostanin S, Fechner M, Parihar S, Maznichenko I V, Mertig I and Kirschner J 2011 *Phys. Rev. Lett.* **106** 087203
[15] Valencia S *et al* 2011 *Nat. Mater.* **10** 753
[16] Borek S, Maznichenko I V, Fischer G, Hergert W, Mertig I, Ernst A, Ostanin S and Chassé A 2012 *Phys. Rev.* B **85** 134432
[17] Lukashev P V, Burton J D, Jaswal S S and Tsymbal E Y 2012 *J. Phys.: Condens. Matter* **24** 226003
[18] Dai J Q, Song Y M and Zhang H 2012 *J. Appl. Phys.* **111** 114301
[19] Lu H *et al* 2012 *Appl. Phys. Lett.* **100** 232904
[20] Tusche C, Meyerheim H L, Jedrecy N, Renaud G, Ernst A, Henk J, Bruno P and Kirschner J 2005 *Phys. Rev. Lett.* **95** 176101

[21] Vaz C A F, Bland J A C and Lauhoff G 2008 *Rep. Prog. Phys.* **71** 056501
[22] Junquera J and Ghosez P 2003 *Nature* **422** 506
[23] Oleinik I I, Tsymbal E Y and Pettifor D G 2001 *Phys. Rev.* B **65** 020401
[24] Polisetty S, Echtenkamp W, Jones K, He X, Sahoo S and Binek C 2010 *Phys. Rev.* B **82** 134419
[25] Kresse G and Hafner J 1994 *Phys. Rev.* B **49** 14251
[26] Kresse G and Furthmüller J 1996 *Phys. Rev.* B **54** 11169
[27] Lüders M, Ernst A, Temmerman W M, Szotek Z and Durham P J 2001 *J. Phys.: Condens. Matter* **13** 8587
[28] Ebert H, Ködderitzsch D and Minár J 2011 *Rep. Prog. Phys.* **74** 096501
[29] Ebert H *et al The Munich SPR-KKR package, version 5.4* available online at http://olymp.cup.uni-muenchen.de/ak/ebert/SPRKKR
[30] Blöchl P E 1994 *Phys. Rev.* B **50** 17953
[31] Perdew J P and Wang Y 1992 *Phys. Rev.* B **45** 13244
[32] Monkhorst H J and Pack J D 1976 *Phys. Rev.* B **13** 5188
[33] Korringa J 1947 *Physica* **13** 392
[34] Kohn W and Rostoker N 1954 *Phys. Rev.* **94** 1111
[35] Guo G Y 1998 *Phys. Rev.* B **57** 10295
[36] Liechtenstein A I, Katsnelson M I, Antropov V P and Gubanov V A 1987 *J. Magn. Magn. Mater.* **67** 65
[37] Razee S S A, Staunton J B and Pinski F J 1997 *Phys. Rev.* B **56** 8082
[38] Fischer G, Däne M, Ernst A, Bruno P, Lueders M, Szotek Z, Temmerman W and Hergert W 2009 *Phys. Rev.* B **80** 014408
[39] Otrokov M M, Ernst A, Ostanin S, Fischer G, Buczek P, Sandratskii L M, Hergert W, Mertig I, Kuznetsov V M and Chulkov E V 2011 *Phys. Rev.* B **83** 155203
[40] Otrokov M M *et al* 2011 *Phys. Rev.* B **84** 144431
[41] Momma K and Izumi F 2011 *J. Appl. Crystallogr.* **44** 1272
[42] Koningsberger D and Prins R (ed) 1988 *X-Ray Absorption: Principles, Applications, Techniques of EXAFS, SEXAFS and XANES* (New York: Wiley)
[43] Stöhr J, Padmore H A, Anders S, Stammler T and Scheinfein M R 1998 *Surf. Rev. Lett.* **5** 1297
[44] van der Laan G 1996 *J. Magn. Magn. Mater.* **156** 99
[45] Lejaeghere K, Van Speybroeck V, Van Oost G and Cottenier S 2014 *Crit. Rev. Solid State Mater. Sci.* **39** 1
[46] Duan C G, Velev J P, Sabirianov R F, Zhu Z, Chu J, Jaswal S S and Tsymbal E Y 2008 *Phys. Rev. Lett.* **101** 137201
[47] Stengel M, Aguado-Puente P, Spaldin N A and Junquera J 2011 *Phys. Rev.* B **83** 235112
[48] Stöhr J and Siegmann H 2006 *Magnetism* (Berlin: Springer)
[49] Kunes J and Oppeneer P 2003 *Phys. Rev.* B **67** 024431